Contents lists available at ScienceDirect

Arabian Journal of Chemistry

journal homepage: www.ksu.edu.sa

Numerical treatment for the desirability of Hall current and activation energy in the enhancement of heat transfer in a nanofluidic system

Muhammad Shoaib [a], Sana Ullah Saqib [b], Kottakkaran Sooppy Nisar [c,*], Muhammad Asif Zahoor Raja [d,*], Imtiaz Ali Mohammed [e]

[a] Yuan Ze University, AI Center, Taoyuan 320, Taiwan
[b] Department of Applied Mathematics and Statistics, Institute of Space Technology, Islamabad, Pakistan
[c] Department of Mathematics, College of science and Humanities in Alkharj, Prince Sattam bin Abdulaziz University, 11942, Saudi Arabia
[d] Future Technology Research Center, National Yunlin University of Science and Technology, 123 University Road, Section.3, Douliou, Yunlin 64002, Taiwan
[e] Department of Chemistry, College of science and Humanities in Alkharj, Prince Sattam bin Abdulaziz University, 11942, Saudi Arabia

ARTICLE INFO

Keywords:
Nanofluid
Hall current
Intelligent computing
Nanoliquid
Nanoparticle aggregation
Binary chemical reaction

ABSTRACT

The growing attractiveness of Artificial Neural Networks (ANNs) derives from their exceptional effectiveness in handling difficult and exceptionally nonlinear mathematical ideas. In complicated disciplines such as fluid mechanics, biological computation, and the field of biotechnology ANNs provide a diverse computing framework that is extremely valuable. This article's major aim is to harness the capabilities of the Levenberg-Marquardt technique with backpropagation intelligent neural networks (LM- BPINNs) to study there is still a lack of clarity regarding the mechanics underlying the increased heat transfer caused by dispersed nanoparticles. The using proposed LM-BPINNs to improve the heat transmission use activation energy and Hall current phenomena in nanofluid (HTAHCNF). The data set is obtained by using Lobatto-III. A method and then ANNs is applied. The LM- BPINNs technique is applied by utilizing reference datasets, with 80% of the dataset devoted to training, 10% to testing, and 10% to verification. The precision/accuracy and converging of developed LM- BPINNs are validated based on the obtained reliability via efficient fitness achieved on mean squared error (MSE), comprehensive regression analysis, and appropriate error histogram visualizations. A diminished MSE indicates that the model's predictions are more reliable. The outcome is consistent with getting a minimal absolute error close to zero, exhibiting the effectiveness of the proposed approach.

1. Introduction

Scientists and investigators seem more interested in Artificial Neural Networks (ANNs) approaches due to its worth and suitableness in treating challenging, stiff, and high nonlinear mathematical models for use in domains like fluid dynamics, computational biology and biotechnology. Researchers are paying a lot of attention to artificial neural networks these days. Because ANN is an artificial intelligence-based technology that might be employed in the categorizing process. According to its many possible applications in microelectronics, transportation, paper manufacture, conductive reducing, and medical qualities, such as heat transmission in muscle, prescription pharmaceutical aiming, and so on, it has a long list of prospective applications. Among the most significant recent AI techniques are artificial neural networks (ANNs). ANNs are ecologically adapted in many circumstances and depending on the understanding that analyses the input throughout the learning experience, whether it originates from inside or beyond the network. A neural network (NN)-based technology is now being designed to learn, identify trends, predict occurrences, and address issues in any corporate entity. A set of algorithms known as neural networks are designed to emulate the brain function and are used to recognize trends. Comparable to computer vision, they categorize or merge raw inputs to comprehend visual information. All real statistics, including pictures, sounds, texts, and timelines, must be converted into the visual statistical patterns known as vectors. Since the invention of the computer, artificial intelligence networks have existed. Mathematicians Warren McCulloch and Walter Pitts created a rotation system in 1943 that used efficient algorithms to simulate how the human brain works. An ANN is composed of a considerable multiprocessor that

Peer review under responsibility of King Saud University.
* Corresponding authors.
E-mail address: n.sooppy@psau.edu.sa (K.S. Nisar).

https://doi.org/10.1016/j.arabjc.2023.105526
Received 19 June 2023; Accepted 4 December 2023
Available online 6 December 2023

Nomenclature

Ω	Angular velocity
f	Fluid
T_w	Uniform Temperature
$J = (J_r, J_\phi, J_z)$	Current density
E = (0, 0, 0)	Electric field,
P_e	Electrical shear
τ_e	Time of an electron collision
n_e	Density of electron
p	pressure
K_r	Reaction rate
C	Concentration
n	Constant fitted rate
δ	Temperature ratio parameter
np	nanoparticle
NFs	Nanofluids
Le	(Lewis number
C_p	Specific heat capacity

Abbreviations

HTAHCNF	heat transmission, use activation energy and Hall current phenomena in nanofluid characteristics
Er.H.As	Error histogram analysis
AI	Artificial intelligence
MSE	Mean square error
NN	Neural Network
ACE	Activation energy
B_0	Magnetic field
U, V, W	Velocity components
c_w	Uniform Concentration
$B = (0, B_0, 0)$	Magnetic induction
D_B	Diffusivity of mass
e	The electron's charge
σ	Electrical conductivity
$m = \omega_e \tau_e$	Hall parameter
T	Temperature
Pr	Prandtl number
Ea	Activation energy coefficient
κ	Boltzmann constant
φ_a	nanoparticle volume fraction
l	Base fluid
nl	Nanoliquid
β	Chemical reaction parameter
D_{nl}	Diffusivity

Abbreviations

LM- BPINNs	Levenberg-Marquardt Technique's with back propagation intelligent neural networks
ANNs	Artificial Neural Networks
AI BP	Back-propagation
R.As	Regression analysis
AE	Absolute error
ArE	Arrhenius equation

operates in parallel and is set up in levels. Because of their famed flexibility, neural networks are constantly adapting as they take in new information from their fundamental training and future running.. Artificial networks can provide a solution to this problem (ANNs). ANNs, modeled on how the brain works, are a different kind of standard programmed computer. Connecting neurons to a network gives neural calculations their power. When more neurons are added to a connected network, it is better to predict the output. ANNs have a broad array of applications because to their unique attributes. A new way for achieving convergence stabilization, the Levenberg-Marquardt (LM) back propagation method for ANNs offers numerical solutions to a wide variety of fluid flow issues. Recently, many scientists have experimented with Newtonian and Non-Newtonian fluid systems using the LM- BPINNs. ANNs are used in a broad spectrum of industries, notably engineering, avionics, pharmaceuticals, the automobile industries, the military, and numerous others (Dubey and Yadava, 2008; Notton et al., 2019). The value of LM- BPINNs is shown by heartbeat Model (Zhang et al., 2021), COVID-19 model (Cheema, 2020), Neuro-fuzzy (Tabbussum and Dar, 2021), the pantograph (Sabir et al., 2022), and differentiated designs (Ilyas et al., 2021; Ilyas et al., 2021; Ahmad et al., 2019; Cheema and Naz, 2021).

A new class of fluids called NFs was created by distributing components with a size of nanometers (nanorods, nanoparticles, nanotubes, nanosheet, or droplets, nanofibers, nanowires) in basic fluids. In other terms, NFs are compressed nanomaterials suspended in nanoscale aggregates. Generally, the nanoparticles are formed of carbon nanotubes, oxides, carbides, or metals. For illustrate, the base fluids include water, ethylene, glycol, oil, and a variety of others. It is noted to possess a number of significant and advantageous characteristics of a NF, including an increase in heat transmission and a NFs rate of stretching. NF coolants are typically utilized to enhance the quality of aerodynamic structures. In comparison to base fluids like water or oil NFs have been discovered to have improved heat capacity, temperature gradient, viscous, and coefficients of convective heat transfer. It has shown excellent promise for use in numerous fields. NFs have gained a significant level of attention in recent years. Numerous applications are the main impetus for NF research. In previous years, nanotechnology has significantly contributed to many heat transmission techniques and made notable advancements in energy-related applications. By enhancing the fluids' characteristics, nanotechnology has significantly advanced the study of heat transmission. Due to the rapid advancement of technologies in all realms of life, the energy requirement is currently constantly rising globally. NFs are essentially improved heat transmission fluids that can be used instead of pure base fluids to enhance heat transport by including nanoparticles substances with better thermally conductivity. NFs are becoming an important component of heat transfers technology because they offer a viable opportunity for improving technology efficiency, which leads to apparatus size reduction and energy savings.

At first, Choi (Choi and Eastman, 1995) concurred with this theory and developed a novel new class of NFs that exhibits a significant thermal conductivity. A NFs flow and heat transmission over a surface that was non - linearly extending were evaluated by Rana and Bhargava (Rana and Bhargava, 2012). Several authors suggested some additional pertinent and unique investigations conducted under various circumstances (Gajbhiye et al., 2023; Jayavel et al., 2023; Oreyeni et al., 2023; Shah et al., 2023; Vemulawada et al., 2023; Özerinç et al., 2010; Rasool et al., 2019; Kumar et al., 2019; Irfan et al., 2019; Khan et al., 2020). Mustafa (Mustafa, 2017) studied the flow of a NF through a rotating disc that was being warmed convectively. Mahanthesh et al. (Mahanthesh et al., 2018) investigated influence of erratic thermal sources on nanoliquid flow. Upadhyaet al. (Abraham, 2018) studied at the thermal transfer attributes of the nanoliquid that was heated internally. Iqbal et al. (Ono and Sakashita, 2010) glanced into the repercussions of carbon nanotubes on the advancement of thermal transport over a revolving surface. They asserted that NPs being suspended increases the flow and heat structure. There is a variety of literature (Afridi et al., 2016; Afridi, n.d.; Afridi et al., 2019; Afridi et al., 2019) about NFs enhanced ability to transmit thermal. Recent advancements from the perspectives of NFs have greatly saturated the domain of fluid

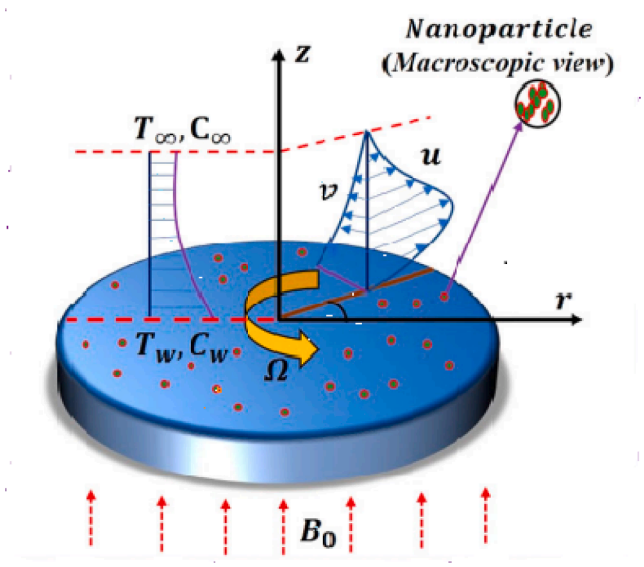

Fig. 1. A graphic illustration of the problem.

mechanics. Darcy's phenomena (Darcy, 1856) are participated in multiple real-world issues and industrial procedures. As an instance, the flow of water through a rugged surface occurs naturally. The physical phenomenon is, in some way, surrounded by the characteristics of permeability. The ensuing drag contribution is generally disregarded for a narrow range for the permeability factor. Because of the wide range of industrial applications, mass and heat transfer across NF flows is a complicated subject for scientists to study. Experimental tests, Fourier's concept (Fourier and Darboux, 1822) of radiant heat is rather restricted as a scientific explanation for the conundrum of heat transfer performance in its usual form. Cattaneo (Cattaneo, 1948) was successful in achieving this goal by incorporating a transient relaxation aspect into the heat transport flux representation. Christov (Christov, 2009) introduced significant mathematical improvements to this heat concept to compensate for the requirement of using the higher convective derivatives within the same situation.

Aggregates are a phenomenon where molecules or particles come together to form lengthy patterns. The aggregation procedure is important in interfacial research and technology since it is an inevitable phenomenon. Amalgamation and aggregating, while on the other side, vary a little. Amalgamation is the arrangement of molecules in a particular sequence with binding interactions, as opposed to loosely coupled agglomeration, which can be destroyed by mechanical force. Via using fractal geometry, this aggregation structure can be recognized. There is much contention about how to increase the thermal conductivity of NFs. Recent research suggests that aggregation of nanomaterial's plays a significant part in the thermal efficiency of NFs. Keblinski et al. (SUS et al., 2002) proposed that size of the particles, nanoparticle aggregation, and liquid-molecule interface represent major enhancing aspects in comparison to the Brownian movement of the particles. The effective heat conductivity produced by Wang et al. (Vassallo et al., 2004) that the aggregation kinematics. Fractal theory helps successfully explain the formation of nanoscale aggregates, as demonstrated by Cai et al. (Fronk and Garimella, 2016). Recent publications (Rana et al., 2021; Mahanthesh, 2021; Mahanthesh et al., 2021) include some initiatives in this direction.

Many technical and industrial procedures make utilization magneto hydrodynamic (MHD) electrically contacting fluid. Flow meters, MHD hydroelectric dams, nuclear reactors, stirrer, and MHD pumping are a few instances. This is important to understanding how the solar cycle and the development of sunspots work in the context of solar physics. Hannes Alfven (Alfvén, 1943) developed the MHD. An instance of MHD uses includes drug carrier aiming, refrigeration of processors built of liquid metal, and crystalline formation. The intensity of magnetic inductions has a significant effect on MHD. Pavlov (Pavlov, 1974) was the first to propose the concept of a highly conductive liquid magnetically flowing from a stretched sheet. The electrolyte solution fluid transient from a pliable surface with a magnetic field has been the subject of discussion by numerous researchers (El-Aziz and Salem, 2007; Akbar et al., 2015; Khan et al., 2016). Even as magnetic field grows greater, the Hall effect, which is brought on by Hall currents, cannot be ignored. In both the Hall acceleration issue and flight MHD, the Hall current is plays a crucial property. The movements of nanoliquid over a rotating disc have been studied by various researchers (Abdel-Wahed and Akl, 2016; Khan et al., 2020; Mahanthesh et al., 2020) using the Hall current approach. However, the Hall current phenomenon in aggregation dynamics is not taken into consideration.

A massive chunk of activation energy (ACE) has always been needed for chemical reactions, whether they are linear or quadratic. The

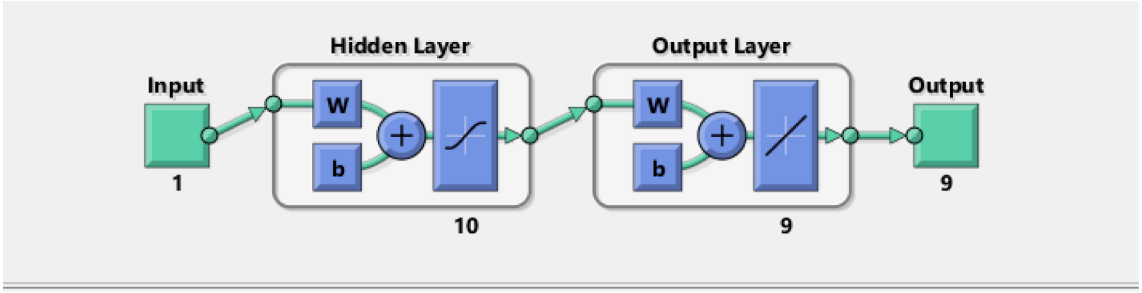

Fig. 2. LM- BPINNs System.

Table 1
Scenarios/cases for Significant Parameters of HTAHCNF.

Scenario	Significant Parameters	$m = 1.5$					$m = 2.0$				
		Case-I	Case-II	Case-III	Case -IV	Case- V	Case-VI	Case-VII	Case-VIII	Case -IX	Case- X
S(I)	M	0.5 $\delta = 0.3$	1.0	1.5	2.0	25	0.5 $\delta = 0.35$	1.0	1.5	2.0	25
S(II)	Le	2 $\beta = 0.2$	3	4	5	6	2 $\beta = 0.3$	3	4	5	6
S(III)	E	0.3	0.9	1.5	2.1	2.7	0.3	0.9	1.5	2.1	2.7

Table 2
Outcomes of LM-BPNNs for all scenarios of HTAHCNF.

Scenario	Case	Mean Square Error			Performance	Mu Parameter	Gradient	Epochs	Time
		Training	Validation	Testing					
S(I)	I	3.22E-08	5.34E-80	3.67E-80	3.23E-08	1.00E-08	1.82E-06	1000	12
	II	3.98E-08	4.23E-08	3.45E-08	3.98E-08	1.00E-08	2.25E-06	943	11
	III	8.12E-07	1.14E-06	5.38E-07	7.92E-07	1.00E-09	1.91E-05	184	2
	IV	4.00E-08	4.93E-08	8.43E-08	4.00E-08	1.00E-05	1.23E-05	1000	5
	V	1.84E-08	2.93E-08	4.39E-08	1.85E-08	1.00E-09	2.77E-07	1000	11
	VI	7.88E-07	1.04E-06	1.04E-06	7.74E-07	1.00E-08	1.65E-06	246	02
	VII	5.34E-08	6.24E-08	5.10E-08	5.35E-08	1.00E-08	9.33E-7	1000	10
	VIII	9.30E-07	8.05E-07	7.78E-07	9.26E-07	1.00E-08	3.48E-06	102	01
	IX	5.10E-07	5.90E-07	4.54E-07	5.10E-07	1.00E-08	2.60E-07	177	01
	X	6.12E-08	9.07E-08	6.90E-08	6.13E-06	1.00E-08	1.16E-06	1000	12
S(II)	I	8.49E-08	1.06E-07	7.73E-08	8.50E-08	1.00E-09	2.29E-06	1000	13
	II	1.29E-06	1.12E-06	9.76E-07	1.02–06	1.00E-07	3. 58E-06	91	01
	III	1.04E-06	8.49E-07	6.54E-07	1.99E-06	1.00E-08	9.97E-06	215	02
	IV	6.77E-08	8.08E-08	4.83E-08	6.78E-08	1.00E-09	3.09E-06	1000	11
	V	1.97E-08	1.83E-08	1.73E-08	1.97E-08	1.00E-09	1.52E-06	938	10
	VI	1.60E-06	1. 31E-06	1.53E-06	1.58E-06	1.00E-07	3.10E-06	938	10
	VII	4.05E-08	5.75E-08	6.51E-08	4.06E-08	1.00E-05	1.33E-05	1000	04
	VIII	9.64E-08	2.08E-07	1.27E-07	9.12E-08	1.00E-08	3.51E-06	480	05
	IX	9.77E-06	9.50E-07	8.12E-06	8.60E-10	1.00E-08	3.74E-08	288	2
	X	2.63E-08	3.19E-08	2.62E-08	2.63E-08	1.00E-08	4.65E-07	1000	11
S(III)	I	1.12E-06	9.40E-07	7.67E-07	1.12E-06	1.00E-08	5.64E-06	186	02
	II	8.29E-07	7.98E-07	1.13E-06	8.62E-07	1.00E-08	8.54E-07	240	02
	III	1.06E-06	1.03E-06	1. 32E-06	1.02E-06	1.00E-07	3.33E-06	89	01
	IV	5.97E-07	6.40E-07	5. 90E-07	5.92E-07	1.00E-09	1.82E-06	355	04
	V	8.47E-07	1.08E-06	8. 83E-07	8.26E-07	1.00E-07	3.01E-06	113	01
	VI	2.48E-08	2.96E-08	3. 21E-08	2.43E-08	1.00E-09	3.35E-05	711	09
	VII	1.14E-06	6.90E-07	6. 03E-06	1.14E-06	1.00E-08	3.10E-06	247	03
	VIII	5.19E-08	7.16E-08	4.37E-08	5.20E-08	1.00E-08	1.82E-06	1000	10
	IX	4.80E-08	1.436E-07	7.54E-08	4.80E-08	1.00E-05	7.22E-06	1000	06
	X	2.85E-08	3.48E-08	2.44E-08	2.85E-08	1.00E-08	3.95E-07	1000	10

Arrhenius equation (ArE) can be used to determine the quantity of ACE in a model that incorporates chemical reactions. ArE describes the internal system temperature change induced on by chemical process. Svante Arrhenius (Herbert, 1907) published the discovery on ACE in 1889 that he described as the level of energy required to react with the least amount of effort. Oil reserves, petrochemical engineering, and geological sciences are a few examples of ACE applications. Abdelmalek et al. (Abdelmalek et al., 2020) investigated the Casson NFs flow behavior beyond an extended surface with a binary chemical process, and they found that a larger ACE increases the concentrations boundary layer's thickness. Kumar et al. (Kumar et al., 2021) explored the significance of improved ArE on MHD for the nanoliquid flow through a spinning surface and how mass transfer rate increases with larger ACE. Mainly focusing on ACE from recently is contained in (Muhammad et al., 2021; Shahid et al., 2021; Bég et al., 2015).

By utilizing LM-BPINNs, the present numerical work helps to create heat transfer converter systems that are more energy efficient, operate better, and also have reduced operational expenses. ANNs can predict complicated and nonlinear interactions, which is important given that most of the other connections between inputs and outputs in real life, both are convoluted and non-linear. The ability of NNs to learn from their errors lets them enhance their performance. As a consequence, NNs are now being employed more frequently to resolve challenging issues. With the help of the artificial neural network (ANN) model created utilizing the experimental observations, optimized results got approximated. The present numerical analysis aids in the development of managed heat ex-changers. techniques that operate better, use less energy, and have reduced running costs. It was reported that the ANN estimator is more precise in comparison to the regression model and experimental data. Patel et al. (GC et al., 2017) have used batching training session to conduct a parameterization analysis to adjust and optimize the neural network model. It is apparent that a numerical method is used to predict the heat transport characteristics of the model as a function of some input parameters Hartman number M. Hall current parameter m, Lewis number Le, temperature difference parameter δ, activation energy E, chemical reaction parameter β and Prandtl number Pr. The artificial neural networks (ANNs) were built using the data generated by statistically calculating these parameters for various parameters. Since this batching training technique required extremely employing responses equations, training data was intentionally produced. Furthermore, an ANN model was constructed and its comprehension were analyzed (reverse mapping) using statistically regression models with the aid of test cases, (forward mapping). The outcomes demonstrated that every ANN model created can produce both backward and backward mapping forecasts that are accurate. R.A, AEA histograms, MSE-based merit, and comparing with the standard solution were used to confirm the accuracy of the ANN scheme used to solve the problem. The ANN model was found to be quite effective in a comparison study that has been done to verify the findings presented here.

The literature mentioned above underlines how AI-based NNs have not yet been applied to predict the heat transport characteristics of a model. The HTAHCNF problem was addressed by the suggested study's authors using LM- BPINNs. Numerous AI-based approaches were applied in the studies (Sabir et al., 2021; Ahmad et al., 2019; Ahmad et al., 2021; Shoaib et al., 2021; Shoaib et al., 2021; Sabir et al., 2020; Shoaib et al., 2019; Sabir et al., 2020; Yang et al., 2020; Çolak, 2021; Shoaib et al., 2022; Shoaib et al., 2021; Shoaib et al., 2021). The Mathematica and MATLAB technologies are used to carry out these numerical calculations. To optimize the HTAHCNF solutions, BNN-LM is implemented. Nobody has used a LM- BPINNs supervised learning on the HTAHCNF model. The evidence suggests that core methods of artificial intelligence are applied in a variety of fields of science and technology. The following are some of the points we addressed in our discussion:

- In this study, LM-BPNNs with a novel methodology or architecture were created for the HTAHCNF model.
- To obtain a more accurate approximation for the HTAHCNF model, a novel application LM-BPNNs is implemented.

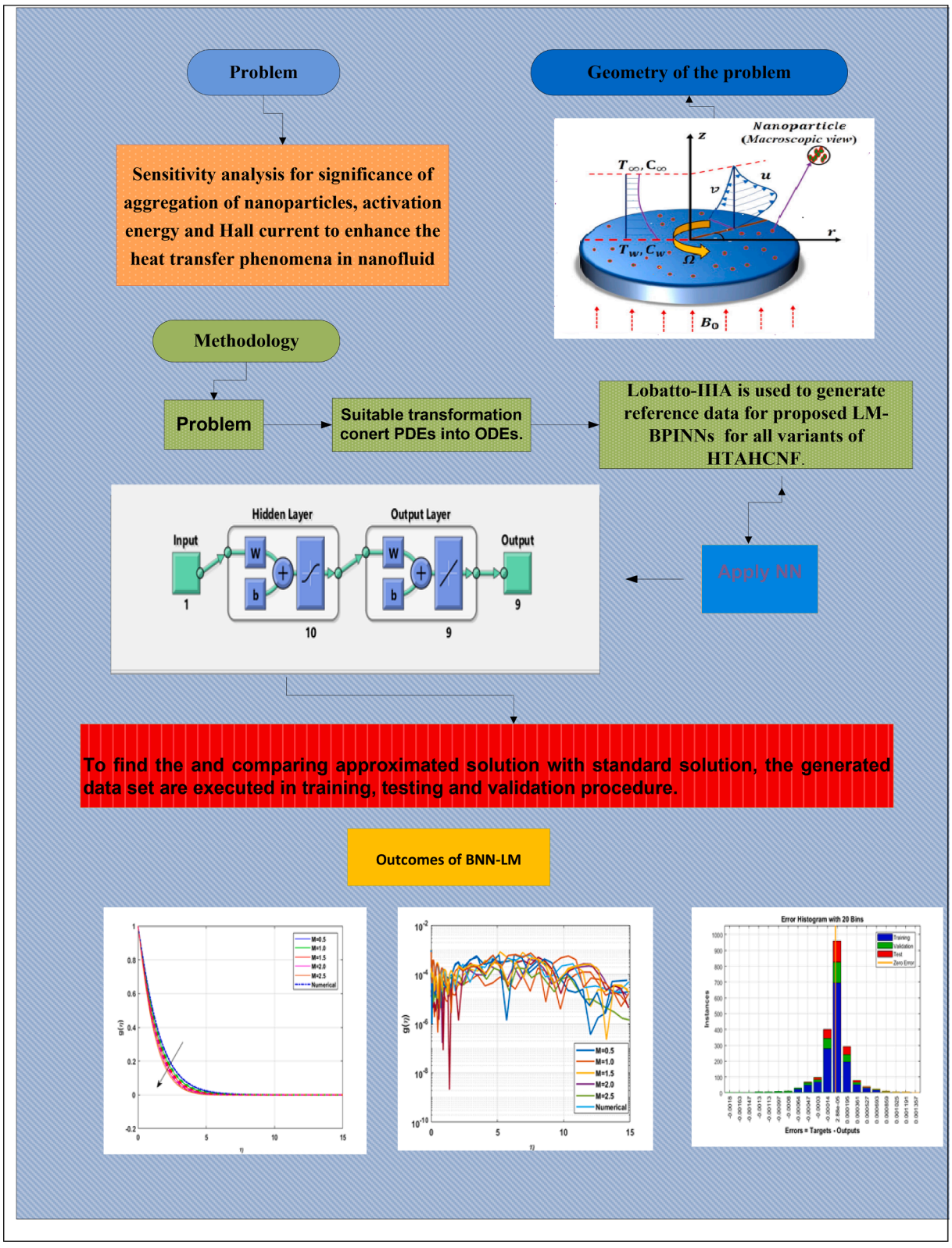

Fig. 3. Flow chart of the presented fluid flow problem LM- BPINNs.

- Developed a set of data from Labatao-IIIA, used it for training, testing, and validation, and compared the result with the accurate solution.
- Model convergence and consistency are displayed on the MSE graph.
- To highlight the great outcome of the LM- BPINNs as demonstrated by fitness curves, MSE, R.A and E.H.A.
- Implications of adding nanoparticle aggregating on the convective heat exchange in ethylene glycol.
- Hall current's influence on nanoparticles' improved heat transfer.
- The influence of ACE on the heat transfer of a nanoliquid as it passes over a disc surface.

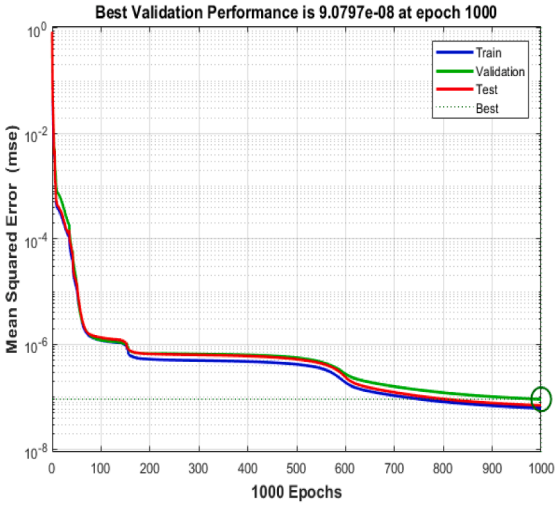

(a). Error via Mean Square of S-I,CX

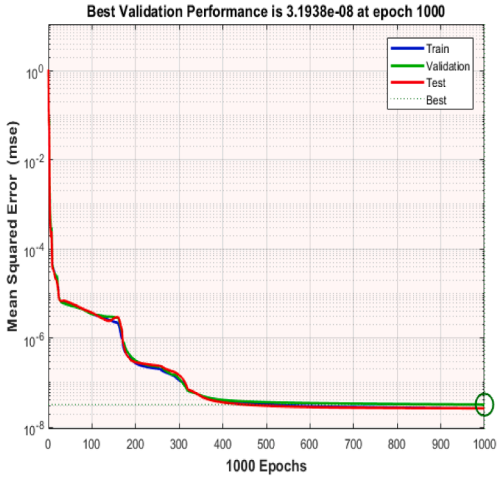

(b). Error via Mean Square of S-II,CX

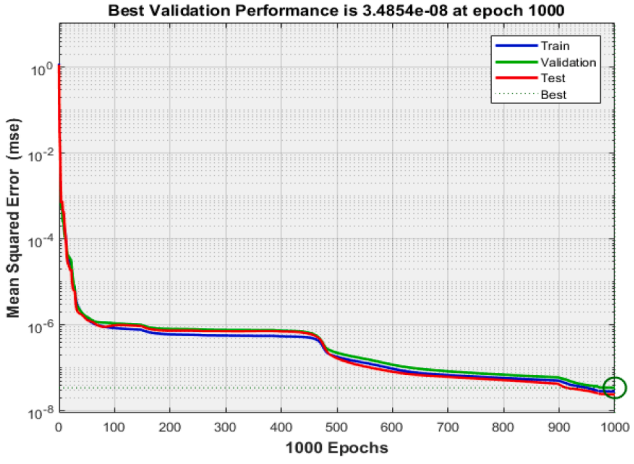

(c). Error via Mean Square of S-III,CX

Fig. 4. Case X of all HTAHCNF scenarios adopting LM-BPNNs Mean Square Error (MSE) representations.

- To construct a quadratic regression model and improve the thermal transfer efficiency, the surface response technique is used with a face-centered central composite system.

The remainder of the article is arranged so that Section 2 offered mathematical modeling, Section 3 contains Solution methodology along with discussion of the study's outcomes, and Section 4 is reserved for concluding remarks and future investigations.

2. Mathematical modeling

It is thought about to explore a time-independent 3D MHD flow of an incompressible, conductive metal nanoliquid (TiO2 based on ethylene glycol) through a rotating disc with a Hall current effect. The disc spins at a uniform rotation speed at $z = 0$. A magnetic field strength B_0 is incorporated in the normal direction of the flow . According to Fig. 1, the flow elements (u, v, w) are orientated in the expanding dimensions (r, z) in a comparable manner. T_W and C_W stand for the surface of the spinning disk's uniform temperature and concentration, respectively, whereas T_∞ and C_∞ indicate the temperatures and concentrations at a distance from the disc surface. The binary chemical reactions and a massive chunk of activation energy are taken into account. Given below is a generalized Ohm's law for NFs in the presence of Hall current (Debnath et al., 1979).

$$(B \times J) \times \frac{\tau_e \omega_e}{B_0} + J = \left(B \times V + \frac{P_e}{en_e} + E\right)\sigma_{nl}\,, \tag{1}$$

here, the electric field magnetic induction, the current density and velocity vectors are denoted by $\boldsymbol{E} = (0,0,0)$, $= (0, B_0, 0)$, $\mathbf{J} = (J_r, J_\phi, J_Z)$ and $\boldsymbol{V} = (u, v, w)$, respectively (Rana et al., 2022):

$$J_r = m_2(mv - u)\frac{\sigma_{nl}B_0}{m_2 + 1},\ J_\phi = (mu + \ \mathrm{v})\frac{\sigma_{nl}B_0}{m_2 + 1}\,, \tag{2}$$

Where $\mathrm{m} = \omega_e\tau_e$ is the Hall parameter, and (u, v, w) are the velocities along the r, ϕ and z directions, respectively.

$$\frac{\partial u}{\partial r} + \frac{\partial w}{\partial z} + \frac{u}{r} = 0, \tag{3}$$

$$\left(\frac{\partial u}{\partial r}u + \frac{\partial u}{\partial z}w - \frac{v^2}{r}\right)\rho_{nl} = \left(\frac{\partial u}{\partial r}\frac{1}{r} + \frac{\partial^2 u}{\partial r} + \frac{\partial^2 u}{\partial z^2} - \frac{u}{r^2}\right)\mu_{nl} + (mv - u)\frac{B_0^2\sigma_{nl}}{(m^2 + 1)}, \tag{4}$$

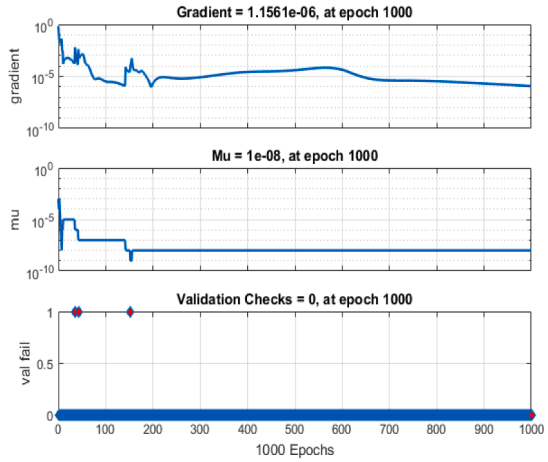

(a). Training state of S-I,C-X

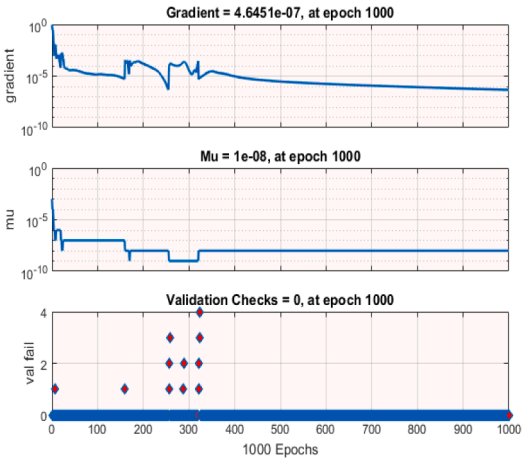

(b). Training state of S-II,C-X

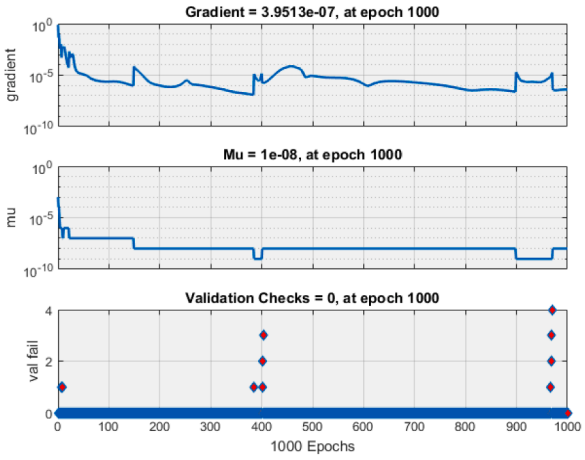

(c). Training state of S-III,C-X

Fig. 5. Display utilizing graphics of the Training state of Case X for all HTAHCNF scenarios.

$$\left(\frac{\partial u}{\partial r}u+\frac{\partial u}{\partial z}w+\frac{uv}{r}\right)\rho_{nl}=\left(\frac{\partial u}{\partial r}\frac{1}{r}+\frac{\partial^2 u}{\partial r}+\frac{\partial^2 u}{\partial z^2}-\frac{v}{r^2}\right)\mu_{nl}-(mu+v)\frac{B_0^2\sigma_{nl}}{(m^2+1)}, \tag{5}$$

$$\frac{\partial p}{\partial z}+\left(\frac{\partial w}{\partial z}w+\frac{\partial w}{\partial r}u\right)\rho_{nl}=\left(\frac{\partial w}{\partial r}\frac{1}{r}+\frac{\partial^2 w}{\partial r}+\frac{\partial^2 w}{\partial z^2}\right)\mu_{nl}, \tag{6}$$

$$\left(\frac{\partial T}{\partial z}w+\frac{\partial T}{\partial r}u\right)(\rho C_p)_{nl}=\left(\frac{\partial T}{\partial r}\frac{1}{r}+\frac{\partial^2 T}{\partial z^2}+\frac{\partial^2 T}{\partial r^2}\right)+k_{nl}, \tag{7}$$

$$\frac{\partial C}{\partial z}w+\frac{\partial C}{\partial r}u=\left(\frac{\partial C}{\partial r}\frac{1}{r}+\frac{\partial^2 C}{\partial z^2}+\frac{\partial^2 C}{\partial r^2}\right)+D_{nl}-K_r^2\exp\left(-\frac{Ea}{kT}\right)\left(\frac{T}{T_\infty}\right)^n(C-C_\infty), \tag{8}$$

Boundary conditions

$$\left.\begin{array}{l} w=0,\ u=0,\ v=\Omega r,\ C=C_w,\ T=T_w\ at z=0 \\ p\to p_\infty,\ u\to 0,\ v\to 0,\ C\to C_\infty,\ T\to T_\infty, as z\to\infty \end{array}\right\}, \tag{9}$$

The NP volume fraction φa is defined as below (Černý, 2017; Alfven, 1943).

$$\varphi_a=\varphi\left(\frac{R_p}{R_a}\right)^{D-3}, \tag{10}$$

As a result, the useful viscous for the aggregating component using the modified KD-model and Eqn. (10) is as follows. (Černý, 2017; Alfven, 1943)

$$\frac{\mu_{nl}}{\mu_l}=\left(1-\frac{\varphi_a}{\varphi_{max}}\right)^{-2.5\varphi_{max}}, \tag{11}$$

Combining the MB-model, the thermal conductivity of the nf is given as follows. (Bruggeman, 1936; Motevasel et al., 2018)

$$\left.\begin{array}{l} k_{nl}=(2\varphi_a(k_a-kl)k_a+2k_l+k_a-\varphi_a(k_a-k_l)+2k_l)k_l, \\ k_a=\frac{k_l}{4}\left[\begin{array}{c}[-1+3(-\varphi_{int}-1)]+\frac{k_{np}}{k_l}(-1+3\varphi_{int})+ \\ \left[\left\{\frac{k_{np}}{k_l}(-1+3\varphi_{int})+(-1+3(-\varphi_{int}+1))\right\}^2+\frac{8k_{np}}{k_l}\right]^{\frac{1}{2}}\end{array}\right], \\ \varphi_{int}=\left(\frac{R_a}{R_p}\right)^{D-3}. \end{array}\right\}, \tag{12}$$

$$\rho_{nl}=\varphi_a\rho_{np}+\rho_l(-\varphi a+1), \tag{13}$$

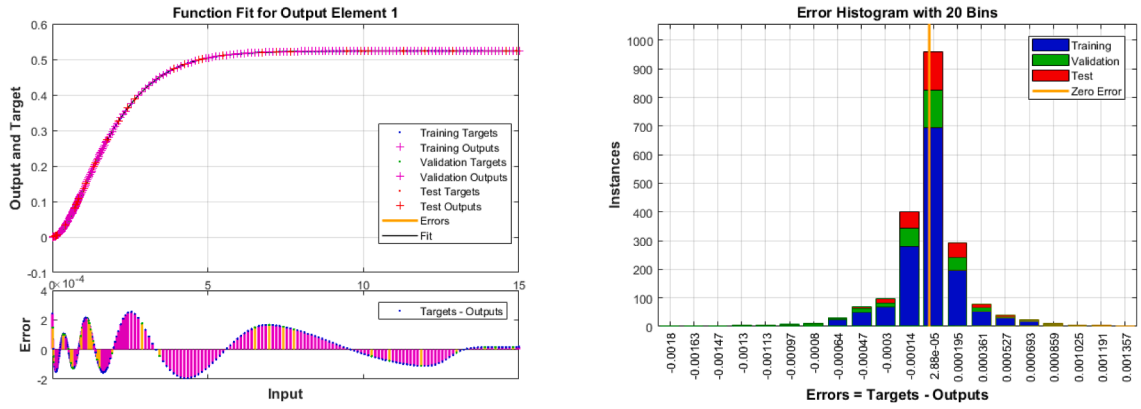

Fitness and Error Histogram Analysis (E.H.A)

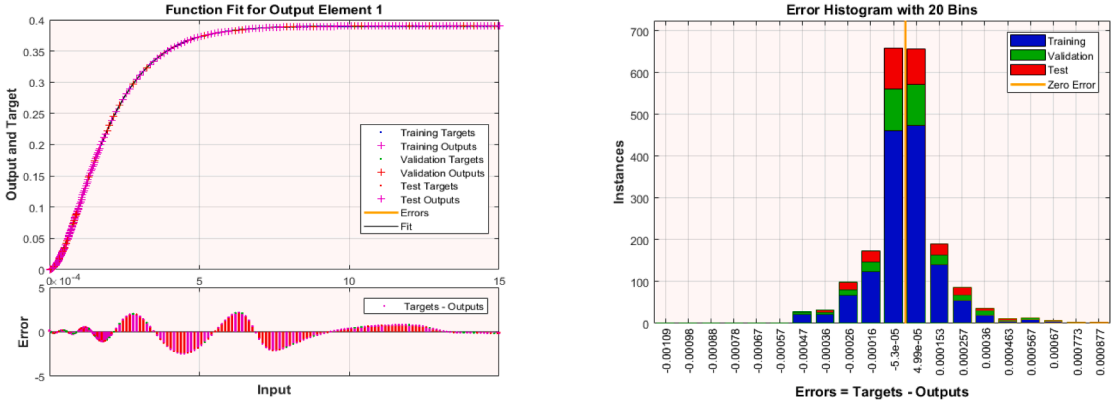

Fitness and Error Histogram Analysis (Er.H.As)

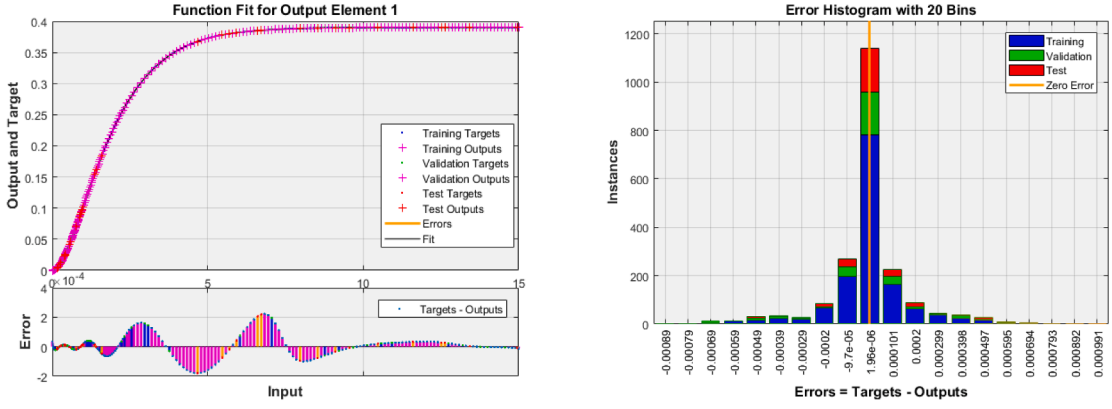

Fitness and Error Histogram Analysis (Er.H.As)

Fig. 6. Comparison of fitness with Er.H.As for case X over all HTAHCNF circumstances utilizing LM-BPNNs.

$$\frac{\sigma_{nl}}{\sigma_l} = 1 + \frac{3\left(-1+\sigma_l\sigma_{np}\right)\varphi_a}{\left(2+\sigma_l\sigma_{np}\right)-\left(-1+\sigma_l\sigma_{np}\right)\varphi_a}\,, \tag{14}$$

$$\left(\rho C_p\right)_{nl} = \varphi_a\left(\rho C_p\right)_{np} + \left(\rho C_p\right)_l\left(-\varphi_a+1\right), \tag{15}$$

$$D_{nl} = D_l\left(-\varphi_a+1\right), \tag{16}$$

Where φ_{int} stands for the NPs volume percent inside the aggregation.. The subscripts n_l, l, a, n_p represent nanoliquid, base liquid, particle aggregation, nanoparticles respectively.

To get a system ODEs, the similarity characteristics in in Eqn. (17) are added in Eqns. (3)-(9) (Abdel-Wahed and Akl, 2016).

$$\left.\begin{aligned} u = \Omega r f'(\eta),\ v = \Omega r g(\eta),\ w = -\sqrt{2\Omega\nu_l f(\eta)},\ \theta(\eta) = \frac{T - T_\infty}{T_w - T_\infty},\\ s(\eta) = \frac{C - C_\infty}{C_w - C_\infty},\ p = p_\infty + 2\Omega\mu_l P(\eta),\ \eta = z\, r\, \sqrt{Re}. \end{aligned}\right\}, \tag{17}$$

The modified system of ODEs with thermo physical characteristics is as follows:

$$\left[g_2 - f^{2'} + 2ff''\right]\frac{A_1}{A_2} - \frac{M}{(m_2+1)}\frac{A_3}{A_2}(f' - mg) + 2f''' = 0, \tag{18}$$

$$\left[-f'g + fg'\right]\frac{2A_1}{A_2} - \frac{M}{(m_2+1)}\frac{A_3}{A_2}(g + mf') + 2g'' = 0, \tag{19}$$

$$\theta'' + \frac{A_4}{A_5}Prf\theta' = 0, \tag{20}$$

$$s'' - \exp\left(-\frac{E}{1+\delta\theta}\right)\frac{(1+\delta\theta)^n}{2A_6}Le\beta sPr + \frac{LePr}{A_6}fs' = 0, \tag{21}$$

$$\left.\begin{aligned} f' = 0, f = 0, g = 1, \theta = 1, s = 1 at \eta = 0\\ f' \to 0, g \to 0, \theta \to 0, s \to 0, as \eta \to \infty \end{aligned}\right\}, \tag{22}$$

Where,

$$A_1 = (1-\varphi_a) + \varphi_a\frac{\rho_a}{\rho_l}, A_2 = \left(1 - \frac{\varphi_a}{\varphi_{max}}\right)^{-2.5\varphi_{max}}, A3 = \left(1 + \frac{3\left(\frac{\sigma_a}{\sigma_l} - 1\right)\varphi_a}{\left(\frac{\sigma_a}{\sigma_l} + 2\right) - \left(\frac{\sigma_a}{\sigma_l} - 1\right)\varphi_a}\right),$$

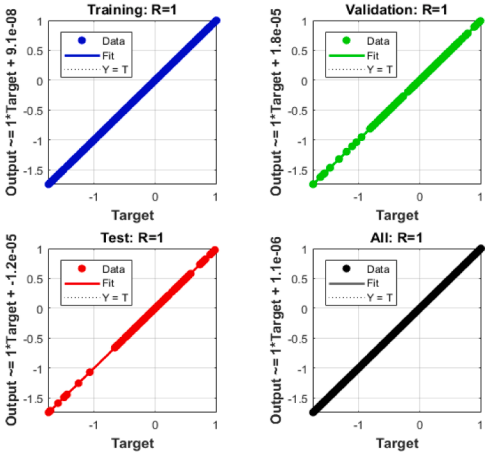

(a) Regression Analysis (R.A) for S-I,C-X

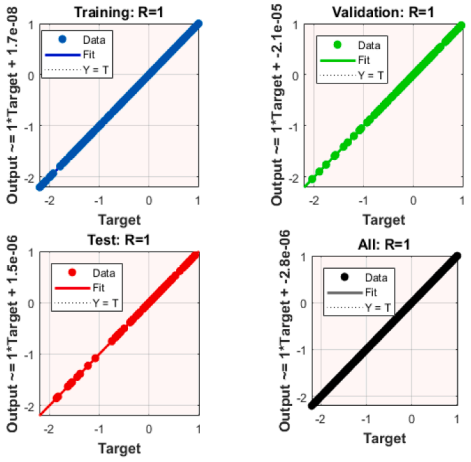

(b). Regression Analysis (R.As) for S-II,C-X

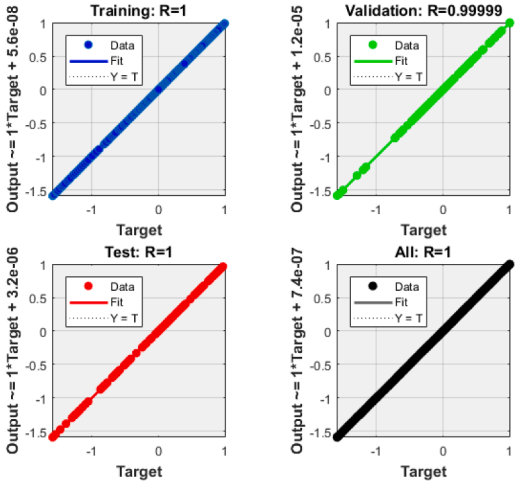

(c). Regression Analysis (R.As) for S-III,C-X

Fig. 7. Utilizing LM-BPNNs, (R.As) of case X of all HTAHCNF scenarios.

$$A_4 = (1-\varphi_a) + \frac{\varphi_a (\rho C_p)_a}{(\rho C_p)_l}, \quad A_5 = \frac{k_{int} + 2k_l + 2\varphi_a (k_{int} - k_l)}{k_{int} + 2k_l - \varphi_a (k_{int} - k_l)}, \quad A6$$
$$= 1 - a \cdot \varphi_a .$$

3. Solution methodology with discussion of outcomes

The Levenberg-Marquardt technique with back propagation neural networks (LM- BPINNs) has been used in the embedded statistical computing system for the HTAHCNF model. The LM- BPINNs driving MATLAB integration toolbox for artificial neural networks is used to solve driven ODEs that describe the flow model in Eqs (18)–(22). Initially, we established a set of data by utilizing the Lobatto III-A numerical solution for the presented flow system containing systems of ODEs, then further utilized for LM- BPINNs. The LM-BPINNs solver is used to analyze the dataset that is generated using the Lobatto III-A numerical technique. Investigation of the evaluation ratio, mean square error (MSE), and absolute error (A.E) using practical data. Using

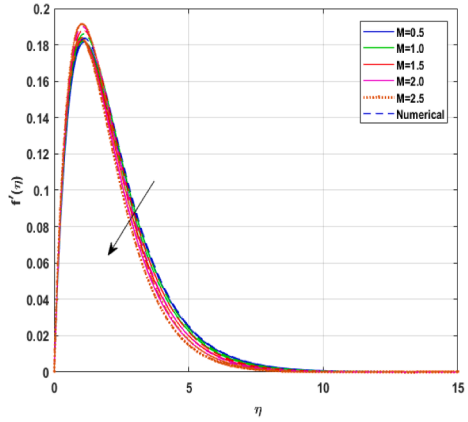

(a). f' for various values of M and m

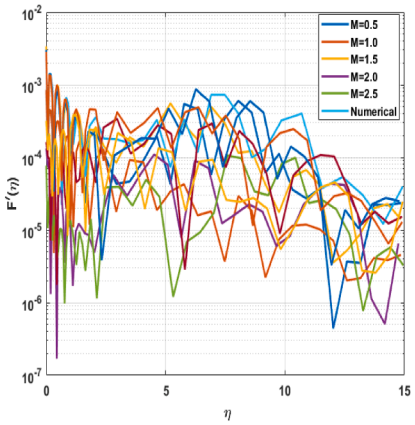

(b). AE representation of M for f'

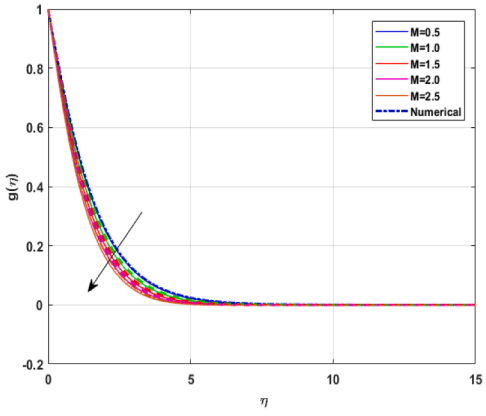

(c). g for various values of M and m

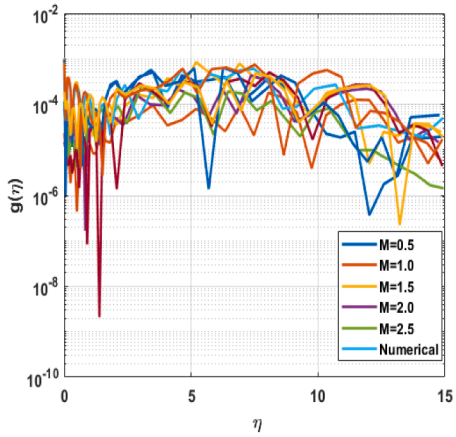

(d). AE representation of M for g

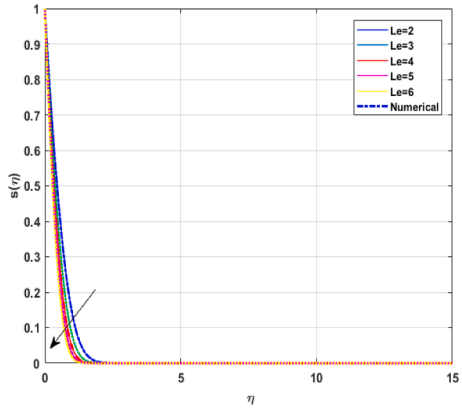

(e). $s(n)$ for various values of Le and δ

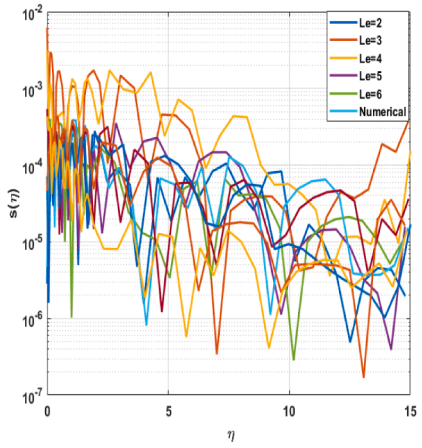

(f). AE representation of $s(n)$ for Le

Fig. 8. The LM-BPNNs result for f' is compared with the corresponding solution, Lobatto III-A Strategy and Outcome A.E analysis.

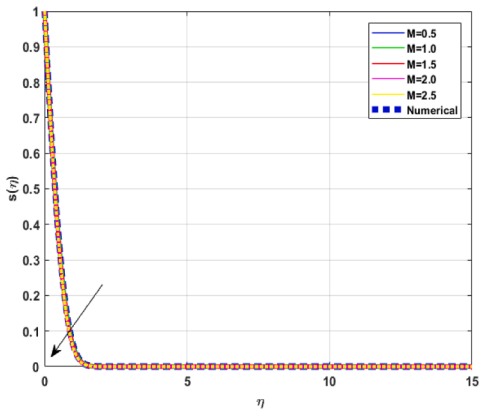

(g). $s(n)$ for various values of M and m

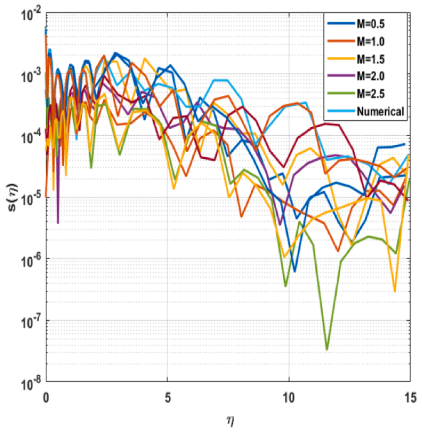

(h). AE representation of $s(n)$ for M

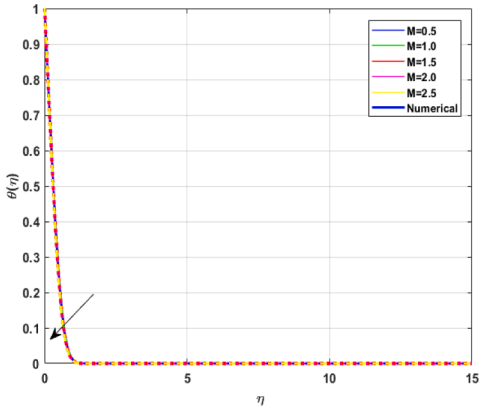

(i) .θ for various values of M and m

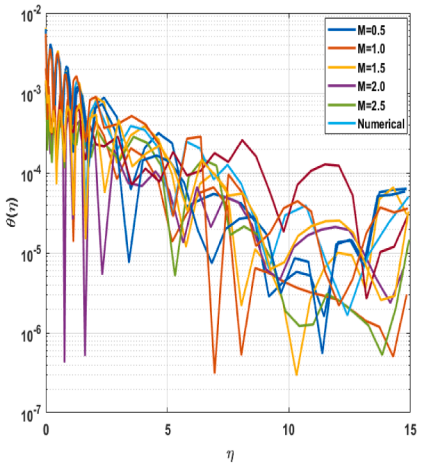

(j). AE representation of M for θ

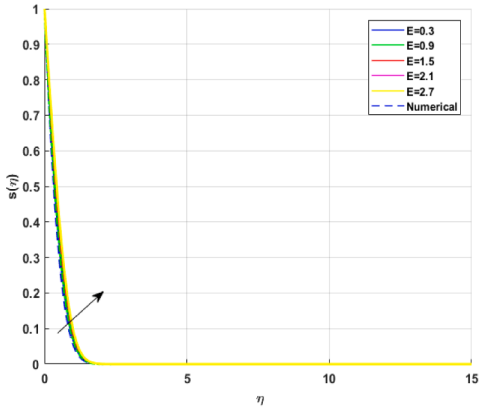

(k). $s(n)$ for various values of E and β

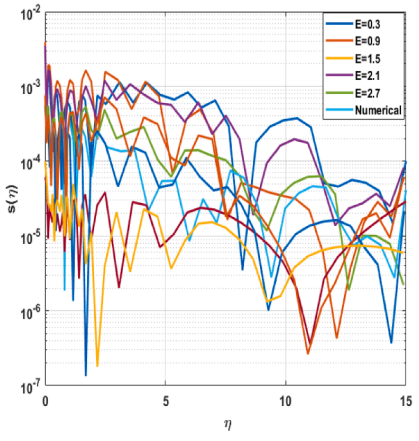

(l). AE representation of $s(n)$ for E

Fig. 8. (*continued*).

the LM- BPINNs paradigm, stability has been achieved via promoting cognitive development. The LM- BPINNs has proven their accuracy and durability by analyzing their results in a number of circumstances and characteristics. A reference set for the networks LM- BPINNs is built between the range [01] of input matrices for Eqs. (18)–(22).

The feed-forward (FF), back-propagation (BP), and multi-layer perceptron (MLP) models are utilized in ANN models. Each node's measurement of the correlation between input data from predecessors forms the foundation of the fundamental learning model. There is only one hidden layer in an MLP network, although a few networks might include more over one. 70 % of the set of data was utilized in the ANN model's training stage, 15 % for the validation stage, and 15 % for the testing stage. The quantity of neurons in the hidden layer isn't determined by a specific model. Because of this, the forecasting abilities of ANN model derived with various numbers of neurons were tested, and the design with 10neurons in the hidden layer was favored. Fig. 2 depicts the design of the constructed ANN models. ANN models employ a variety of training procedures, and numerous researchers (Çolak, 2021) on the

effectiveness of these algorithms have been performed. The constructed model employs one of the elevated classification algorithms, the Levenberg-Marquardt classification model.

Through the discovery of correlations and trends in data, ANNs acquire (or are training). Programming does not help them learn or get training. During training, the inter-unit connection is continually improved until the prediction error is diminished and the system achieves the target precision. Information that aids in your search for the proper solutions carries a lot of weight. Comparable processing abilities imply that a network is capable of doing multiple tasks simultaneously. The entire system stores information, rather than only on the website, or network. Reading and imitating indirect, intricate relationships requires the capacity to imitate interpersonal interaction in the real world. Information is stored throughout the network, not just on the website. The ability to read and mimic indirect, complex interactions helps to mimic real-world interactive relationships. The capacity to create output with insufficient information, with loss in performance proportional to the significance of the incomplete details. Mechanical learning means the ability of the neural network artificial (ANN) to learn from events and make judgments based on that awareness. ANNs can anticipate the effect of intangible data because of their productivity and mean invisible association of intangible data. Neural networks are a magnificent biomimetic programming technique that allows a computer to adapt from data collected through observation. Many challenges in image identification, audio identification, and natural language processing may now be solved using neural networks and deep learning.

The set of design variables is considered to be $0.5 \leq M \leq 2.5, 0.2 \leq m \leq 2.0,\ 0.3 \leq \delta \leq 0.5,\ 0.3 \leq E \leq 2.7,\ 0.2 \leq \beta \leq 0.4,\ 2 \leq Le \leq 6$. The variables are used as follows for graphical interpretation $M = 1.5, m = 0.5, \delta = 0.3, n = 0.4, E = 0.9, \beta = 0.2$, and $Le = 3$ excluding the distinctive one.

When constructing the data set for LM- BPNNs, the 3 distinct scenarios are described, and the disparities are for various parameters M m, Le , δ, (ACE) E, chemical β and Pr.

The three scenarios are described in Table.1, while the non-variable parameters of the outcomes are presented in Table 2. Fig. 3 depicted the structure of proposed techniques…..Fig. 4 demonstrates the training effectiveness in each 10th case of the LM-BPNNs scenarios. It can be observed from the figs that the MSE values, which are higher during the start of the training phase, get lower as the epochs advance. According to the MLP network's functioning structure, MSE values decline throughout each epoch, and whenever the minimal MSE value is attained, the ANN model's training phase is accomplished and the best efficiency is obtained. Extremely modest MSE values demonstrate that the constructed ANN models' training stages were successfully ended with extremely minimal error rates. Fig. 5 shows a visualization of the training state of ANN model. Examining the graphs reveals that as the epoch's increases, the values of μ and gradient drop. These graph-based results demonstrate that the training stages of the ANN models are successfully finished. Error histogram analysis is fundamental when assessing the effectiveness of ANN models. Fig. 6 shows the fitness and Er.H. As. The erroneous rates acquired for every data set are shown to be close to the zero erroneous line when the graphs are viewed. It is evident, though, that the statistical values of the errors depicted on the graphs' x-axis are also quite small. These findings from E.H.A. graphs demonstrate that the ANN models were trained with an extremely minimal error rate. The R.As graphs are shown in Fig. 7. By checking and analyzing the training data, the trustworthiness of LM- BPINNs is confirmed for the HTAHCNF design, and according to one's testimony, optimum modeling is shown by a correlation R value that is close to unity. Table. 2 shows the training, testing, validation, performance, Mu, epochs, and total time. The effectiveness of the LM-BPNNs and the veracity of the generated HTAHCNF in each scenario determined the techniques' outcomes..

4. Results and discussion

The radial velocity $f'(\eta)$, transversal velocity g(η), temperature θ (η), and concentration s(η) shows in Fig. 8 (a,c,i,g) the fluctuation caused by an raise in the Hartman number M and the Hall current parameter m. Fig. 8 (a,c,i,g). It has been found that an enhanced M increases the magnitude of the $f'(\eta)$, g(η), θ(η), and s(η) profiles to decline. The Lorentz force (L.F), which is generated by the magnetic field, has an impact on the M. As M is raised, the resistant L.F, which causes friction between the fluid and the surface and lowers velocities increases. A rise in the value of m causes the thermal and concentrating fields to enlarge. The A. E for M and m on $f'(\eta)$, g(η), θ (η), and s(η) shown in Fig. 8 (b,d,j,h) ranging from 10^{-2} to 10^{-7}, 10^{-2} to 10^{-10}, 10^{-2} to 10^{-7} and 10^{-2} to 10^{-8}.

The influence of Le and δ on the concentrating distribution $s(\eta)$ is shown in Fig. 8 (e). It has been found that an drop in $s(\eta)$ field is caused by enhancing Le and δ because mass diffusivity is decreased. Fig. 8 (k). shows the impact of $(ACE)E$ and β on the concentration field. Here, as the A.E rises, the modified Arrhenius function diminishes. In the result, this produces a beneficial chemical reaction that raises the $s(\eta)$. In addition, the relationship between the chemical reaction parameter and the concentration boundary layer is reversed. The A.E for Le and δ on s (η) shown in Fig. 8 (f) ranging from 10^{-2} to 10^{-7}. The A.E for E and β on s (η) shown in Fig. 8 (f) ranging from 10^{-2} to 10^{-7}.

5. Conclusion and future studies

In this research, we provide an AI-based computational design that solves the mathematical model corresponding to the investigation of HTAHCNF for different scenarios by using application LM-BPNNs. This research explored a 3D-MHD flow of the nanoliquid over a spinning disc with NPs aggregating is computationally investigated by providing for Hall current and binary chemical reactions. The Lobatto-IIIA numerical solver is used to generate HTAHCNF reference data by altering Hartman number M,Hall current parameter (m) Lewis number Le, temperature difference parameter δ, activation energy E, Prandtl number Pr. and chemical reaction parameter β using data sets for various flow scenarios. 70 % of the set of data was utilized in the ANN model's training stage, 15 % for the validation stage, and 15 % for the testing stage. The remarkable consistency of proposed results with reference solutions and the accuracy of 10^{-2} to 10^{-10} show the framework's applicability is produced for each scenario in the HTAHCNF in all 10th cases.

- The M is directly proportional to the thickness of the momentum layer structure, which has an inverse relationship to the magnetic field.
- The magnetic field and the M are inversely related to the concentration and temperature layer structure.
- δ and chemical reaction are negatively related to the raise of the concentration layer structure.
- A chemical reaction that is more successful and enhances the concentration layer is caused by higher activation energy.
- The outcomes of the MSE, H.E.A and R. A computations used to evaluate the effectiveness of the ANN design model by HTAHCNF for the ability to forecast with great precision.
- A smaller MSE demonstrates that the model's predictions are more reliable.
- It is observed that the error margins obtained for model is extremely low values.
- Achieved results have demonstrated that the created ANN models can forecast HTAHCNF values with extraordinarily low error margins and high reliability.
- The result is consistent to achieving a minimal absolute error near to zero, proving the significance of the proposed technique.

Future research on the improvement of varying factors using the ANN model can be used to examine the effectiveness of different flow patterns. The results of this investigation have inherent worth for future research endeavors because they experimentally illustrated the analytical implications of using computer models in the scientific literature. The work contributes to a better understanding of the application and efficiency of these theoretical strategies in addressing challenging scientific challenges by proving their efficacy. Furthermore, LM-BPNNs can be used to solve a variety of challenges (Bukhari et al., 2023; Hsu et al., 2023; Fang et al., 2019; Anwar et al., 2023).

Declaration of competing interest

The authors declare that they have no known competing financial interests or personal relationships that could have appeared to influence the work reported in this paper.

Acknowledgement

“ This study is supported via funding from Prince Sattam bin Abdulaziz University project number (PSAU/2023/R/1444) ”

References:

Abdelmalek, Z., Mahanthesh, B., Basir, M.F.M., Imtiaz, M., Mackolil, J., Khan, N.S., Nabwey, H.A., Tlili, I., 2020. Mixed radiated magneto Casson fluid flow with Arrhenius activation energy and Newtonian heating effects: Flow and sensitivity analysis. Alex. Eng. J. 59 (5), 3991–4011.

Abdel-Wahed, M., Akl, M., 2016. Effect of hall current on MHD flow of a nanofluid with variable properties due to a rotating disk with viscous dissipation and nonlinear thermal radiation. AIP Adv. 6 (9), 095308.

Abraham, A.P., 2018. JD and Mohanraj, M., Thermodynamic performance of automobile air conditioners working with R430A as a drop-in substitute to R134a. *Journal of Thermal Analysis and Calorimetry*, *136*(5), pp.2071-2086.

Afridi, M.I., Qasim, M., Khan, I., Shafie, S., Alshomrani, A.S., 2016. Entropy generation in magnetohydrodynamic mixed convection flow over an inclined stretching sheet. Entropy 19 (1), 10.

Afridi, M.I., Qasim, M., Khan, N.A., Hamdani, M., 2019. Heat transfer analysis of Cu–Al2O3–water and Cu–Al2O3–kerosene oil hybrid nanofluids in the presence of frictional heating: using 3-stage Lobatto IIIA formula. J. Nanofluids 8 (4), 885–891.

Afridi, M.I., Qasim, M., Wakif, A., Hussanan, A., 2019. Second law analysis of dissipative nanofluid flow over a curved surface in the presence of Lorentz force: Utilization of the Chebyshev–Gauss–Lobatto spectral method. Nanomaterials 9 (2), 195.

Afridi, C., study and entropy generation analysis of Cu–H2O and Ag–H2O nanofluids flow over a slendering stretching surface, J.

Ahmad, I., Ilyas, H., Urooj, A., Aslam, M.S., Shoaib, M., Raja, M.A.Z., 2019. Novel applications of intelligent computing paradigms for the analysis of nonlinear reactive transport model of the fluid in soft tissues and microvessels. Neural Comput. & Applic. 31 (12), 9041–9059.

Ahmad, I., Raja, M.A.Z., Ramos, H., Bilal, M., Shoaib, M., 2021. Integrated neuro-evolution-based computing solver for dynamics of nonlinear corneal shape model numerically. Neural Comput. & Applic. 33 (11), 5753–5769.

Akbar, N.S., Ebaid, A., Khan, Z.H., 2015. Numerical analysis of magnetic field effects on Eyring-Powell fluid flow towards a stretching sheet. J. Magn. Magn. Mater. 382, 355–358.

Alfven, H., 1943. On the existence of electromagnetic-hydromagnetic waves. *Arkiv. Mat. Astron. Fys.*

Alfvén, H., 1943. On the existence of electromagnetic-hydromagnetic waves. *Arkiv. Mat. Astron. Fys.*

Anwar, N., Ahmad, I., Fatima, A., Kiani, A.K., Shoaib, M., Raja, M.A.Z., 2023. Design of intelligent Bayesian supervised predictive networks for nonlinear delay differential systems of avian influenza model. Eur. Phys. J. Plus 138 (10), 911.

Bég, O.A., Mabood, F., Islam, M.N., 2015. Homotopy simulation of nonlinear unsteady rotating nanofluid flow from a spinning body. Int. J. Eng. Math. 2015, 1–15.

Bruggeman, D.A.G., 1936. Berechnung verschiedener physikalischer Konstanten von heterogenen Substanzen. II. Dielektrizitätskonstanten und Leitfähigkeiten von Vielkristallen der nichtregulären Systeme. Ann. Phys. 417 (7), 645–672.

Bukhari, A.H., Raja, M.A.Z., Alquhayz, H., Abdalla, M.Z., Alhagyan, M., Gargouri, A. and Shoaib, M., 2023. Design of intelligent hybrid NAR-GRNN paradigm for fractional order VDP chaotic system in cardiac pacemaker with relaxation oscillator. *Chaos, Solitons & Fractals*, *175*, p.114047.-order nonlinear multi-singular Emden–Fowler equation. *The European Physical Journal Plus*, *135*(5), p.410.

Cattaneo, C., 1948. Sulla conduzione del calore. Atti Sem. Mat. Fis. Univ. Modena 3, 83–101.

Černý, A., 2017. Solutions to the multi-dimensional Prouhet–Tarry–Escott problem resulting from composition of balanced morphisms. Inf. Comput. 253, 424–435.

Cheema, T.N., et al., 2020. Intelligent computing with Levenberg–Marquardt artificial neural networks for nonlinear system of COVID-19 epidemic model for future generation disease control. Eur. Phys. J. Plus 135 (11), 1–35.

Cheema, T.N., Naz, S., 2021. Numerical computing with Levenberg–Marquardt backpropagation networks for nonlinear SEIR Ebola virus epidemic model. AIP Adv. 11 (9), 095205.

Choi, S.U. and Eastman, J.A., 1995. *Enhancing thermal conductivity of fluids with nanoparticles* (No. ANL/MSD/CP-84938; CONF-951135-29). Argonne National Lab. (ANL), Argonne, IL (United States).

Christov, C.I., 2009. On frame indifferent formulation of the Maxwell-Cattaneo model of finite-speed heat conduction. Mech. Res. Commun. 36 (4), 481–486.

Çolak, A.B., 2021. Experimental analysis with specific heat of water-based zirconium oxide nanofluid on the effect of training algorithm on predictive performance of artificial neural network. Heat Transf. Res. 52 (7).

Darcy, H., 1856. The public fountains of the city of Dijon. Victor Dalmont, Paris, France.

Debnath, L., Ray, S.C., Chatterjee, A.K., 1979. Effects of Hall current on unsteady hydromagnetic flow past a porous plate in a rotating fluid system. Z. Angew. Math. Mech. 59, 469–471.

Dubey, A.K., Yadava, V., 2008. Laser beam machining—A review. Int. J. Mach. Tool Manu. 48 (6), 609–628.

El-Aziz, M.A., Salem, A.M., 2007. MHD-mixed convection and mass transfer from a vertical stretching sheet with diffusion of chemically reactive species and space-or temperature-dependent heat source. Can. J. Phys. 85 (4), 359–373.

Fang, S.H., Li, C.C., Lu, W.C., Xu, Z., Chien, Y.R., 2019. Enhanced device-free human detection: Efficient learning from phase and amplitude of channel state information. IEEE Trans. Veh. Technol. 68 (3), 3048–3051.

Fourier, J.B.J. and Darboux, G., 1822. *Théorie analytique de la chaleur* (Vol. 504). Paris: Didot.

Fronk, B.M., Garimella, S., 2016. Condensation of carbon dioxide in microchannels. Int. J. Heat Mass Transf. 100, 150–164.

Gajbhiye, S., Warke, A., Ramesh, K., 2023. Mathematical modeling and analysis of immiscible metallic based nanofluid flow in a microchannel with non-spherical nanoparticles. Math. Comput. Simul.

GC, M.P., Shettigar, A.K., Krishna, P. and Parappagoudar, M.B., 2017. Back propagation genetic and recurrent neural network applications in modelling and analysis of squeeze casting process. *Applied Soft Computing*, *59*, pp.418-437.

Herbert, F., 1907. Über die adsorption in lösungen. Z. Phys. Chem. 57, 385–470.

Hsu, H.P., Jiang, Z.R., Li, L.Y., Tsai, T.C., Hung, C.H., Chang, S.C., Wang, S.S., Fang, S.H., 2023. Detection of audio tampering based on electric network frequency signal. Sensors 23 (16), 7029.

Ilyas, H., Ahmad, I., Raja, M.A.Z., Shoaib, M., 2021. A novel design of Gaussian WaveNets for rotational hybrid nanofluidic flow over a stretching sheet involving thermal radiation. Int. Commun. Heat Mass Transf. 123, 105196.

Ilyas, H., Ahmad, I., Raja, M.A.Z., Tahir, M.B., Shoaib, M., 2021. Intelligent networks for crosswise stream nanofluidic model with Cu–H2O over porous stretching medium. Int. J. Hydrogen Energy.

Irfan, M., Farooq, M.A., Iqra, T., 2019. Magnetohydrodynamic free stream and heat transfer of nanofluid flow over an exponentially radiating stretching sheet with variable fluid properties. Front. Phys. 7, 186.

Jayavel, P., Ramzan, M., Saleem, S., Verma, A., Ramesh, K., 2023. Homotopy analysis on the bio-inspired radiative magnesium and iron oxides/blood nanofluid flow over an exponential stretching sheet. Comput. Part. Mech. 1–21.

Khan, M., Hussain, M., Azam, M., 2016. Magnetohydrodynamic flow of Carreau fluid over a convectively heated surface in the presence of non-linear radiation. J. Magn. Magn. Mater. 412, 63–68.

Khan, M., Ali, W., Ahmed, J., 2020. A hybrid approach to study the influence of Hall current in radiative nanofluid flow over a rotating disk. Appl. Nanosci. 10 (12), 5167–5177.

Khan, S.A., Nie, Y., Ali, B., 2020. Multiple slip effects on MHD unsteady viscoelastic nano-fluid flow over a permeable stretching sheet with radiation using the finite element method. SN Appl. Sci. 2 (1), 1–14.

Kumar, R., Bhattacharyya, A., Seth, G.S., Chamkha, A.J., 2021. Transportation of magnetite nanofluid flow and heat transfer over a rotating porous disk with Arrhenius activation energy: Fourth order Noumerov’s method. Chin. J. Phys. 69, 172–185.

Kumar, B., Seth, G.S., Nandkeolyar, R., 2019. Regression model and successive linearization approach to analyse stagnation point micropolar nanofluid flow over a stretching sheet in a porous medium with nonlinear thermal radiation. Phys. Scr. 94 (11), 115211.

Mahanthesh, B., 2021. Flow and heat transport of nanomaterial with quadratic radiative heat flux and aggregation kinematics of nanoparticles. Int. Commun. Heat Mass Transf. 127, 105521.

Mahanthesh, B., Gireesha, B.J., Shehzad, S.A., Rauf, A., Kumar, P.S., 2018. Nonlinear radiated MHD flow of nanoliquids due to a rotating disk with irregular heat source and heat flux condition. Phys. B Condens. Matter 537, 98–104.

Mahanthesh, B., Gireesha, B.J., Shehzad, S.A., Ibrar, N., Thriveni, K., 2020. Analysis of a magnetic field and Hall effects in nanoliquid flow under insertion of dust particles. Heat Transfer 49 (3), 1632–1648.

Mahanthesh, B., Thriveni, K., Rana, P., Muhammad, T., 2021. Radiative heat transfer of nanomaterial on a convectively heated circular tube with activation energy and

nanoparticle aggregation kinematic effects. Int. Commun. Heat Mass Transf. 127, 105568.
Motevasel, M., Nazar, A.R.S. and Jamialahmadi, M., 2018. The effect of nanoparticles aggregation on the thermal conductivity of nanofluids at very low concentrations: experiment.
Muhammad T, Waqas H, Khan SA, et al. Significance of nonlinear thermal radiation in 3D Eyring–Powell nanofluid flow with Arrhenius activation energy. J Therm Anal Calorim. 2021;143(2):929–944. DO.
Mustafa, M., 2017. MHD nanofluid flow over a rotating disk with partial slip effects: Buongiorno model. Int. J. Heat Mass Transf. 108, 1910–1916.
Notton, G., Voyant, C., Fouilloy, A., Duchaud, J.L., Nivet, M.L., 2019. Some applications of ANN to solar radiation estimation and forecasting for energy applications. Appl. Sci. 9 (1), 209.
Ono, A. and Sakashita, H., 2010. Temperature measurements near a heating surface at high heat fluxes in subcooled pool boiling. *Heat Transfer—Asian Research: Co-sponsored by the Society of Chemical Engineers of Japan and the Heat Transfer Division of ASME*, *39*(1), pp.27-42.
Oreyeni, T., Oladimeji Akindele, A., Martins Obalalu, A., Olakunle Salawu, S. and Ramesh, K., 2023. Thermal performance of radiative magnetohydrodynamic Oldroyd-B hybrid nanofluid with Cattaneo–Christov heat flux model: Solar-powered ship application. *Numerical Heat Transfer, Part A: Applications*, pp.1-19.
Özerinç, S., Kakaç, S., Yazıcıoğlu, A.G., 2010. Enhanced thermal conductivity of nanofluids: a state-of-the-art review. Microfluid. Nanofluid. 8 (2), 145–170.
Pavlov, K.B., 1974. Magnetohydrodynamic flow of an incompressible viscous fluid caused by deformation of a plane surface. Magnitnaya Gidrodinamika 4 (1), 146–147.
Rana, P., Bhargava, R., 2012. Flow and heat transfer of a nanofluid over a nonlinearly stretching sheet: a numerical study. Commun. Nonlinear Sci. Numer. Simul. 17 (1), 212–226.
Rana, P., Mahanthesh, B., Mackolil, J., Al-Kouz, W., 2021. Nanofluid flow past a vertical plate with nanoparticle aggregation kinematics, thermal slip and significant buoyancy force effects using modified Buongiorno model. Waves Random Complex Media 1–25.
Rana, P., Mahanthesh, B., Thriveni, K., Muhammad, T., 2022. Significance of aggregation of nanoparticles, activation energy, and Hall current to enhance the heat transfer phenomena in a nanofluid: a sensitivity analysis. Waves Random Complex Media 1–23.
Rasool, G., Shafiq, A., Khalique, C.M., Zhang, T., 2019. Magnetohydrodynamic Darcy-Forchheimer nanofluid flow over a nonlinear stretching sheet. Phys. Scr. 94 (10), 105221.
Sabir, Z., Raja, M.A.Z., Umar, M., Shoaib, M., 2020. Design of neuro-swarming-based heuristics to solve the third-order nonlinear multi-singular Emden-Fowler equation. Eur. Phys. J. Plus 135 (5), 410.
Sabir, Z., Raja, M.A.Z., Umar, M., Shoaib, M., 2020. Neuro-swarm intelligent computing to solve the second-order singular functional differential model. Eur. Phys. J. Plus 135 (6), 1–19.
Sabir, Z., Baleanu, D., Shoaib, M., Raja, M.A.Z., 2021. Design of stochastic numerical solver for the solution of singular three-point second-order boundary value problems. Neural Comput. & Applic. 33 (7), 2427–2443.
Sabir, Z., Wahab, H.A., Guirao, J.L., 2022. A novel design of Gudermannian function as a neural network for the singular nonlinear delayed, prediction and pantograph differential models. Math. Biosci. Eng. 19 (1), 663–687.
Shah, N.A., Koriko, O.K., Ramesh, K., Oreyeni, T., 2023. Rheology of bioconvective stratified Eyring-Powell nanofluid over a surface with variable thickness and homogeneous-heterogeneous reactions. Biomass Convers. Biorefin. 1–17.
Shahid, A., Huang, H.L., Khalique, C.M., Bhatti, M.M., 2021. Numerical analysis of activation energy on MHD nanofluid flow with exponential temperature-dependent viscosity past a porous plate. J. Therm. Anal. Calorim. 143 (3), 2585–2596.
Shoaib, M., Akhtar, R., Khan, M.A.R., Rana, M.A., Siddiqui, A.M., Zhiyu, Z. and Raja, M. A.Z., 2019. A novel design of three-dimensional MHD flow of second-grade fluid past a porous plate. *Mathematical Problems in Engineering*, *2019*.
Shoaib, M., Zubair, G., Nisar, K.S., Raja, M.A.Z., Khan, M.I., Gowda, R.P., Prasannakumara, B.C., 2021. Ohmic heating effects and entropy generation for nanofluidic system of Ree-Eyring fluid: Intelligent computing paradigm. Int. Commun. Heat Mass Transf. 129, 105683.
Shoaib, M., Raja, M.A.Z., Sabir, M.T., Bukhari, A.H., Alrabaiah, H., Shah, Z., Kumam, P., Islam, S., 2021. A stochastic numerical analysis based on hybrid NAR-RBFs networks nonlinear SITR model for novel COVID-19 dynamics. Computer.
Shoaib, M., Kausar, M., Khan, M.I., Zeb, M., Gowda, R.P., Prasannakumara, B.C., Raja, M. A.Z., 2021. Intelligent backpropagated neural networks application on Darcy-Forchheimer ferrofluid slip flow system. Int. Commun. Heat Mass Transf. 129, 105730.
Shoaib, M., Raja, M.A.Z., Khan, M.A.R., Farhat, I., Awan, S.E., 2021. Neuro-computing networks for entropy generation under the influence of MHD and thermal radiation. Surf. Interfaces 25, 101243.
Shoaib, M., Kausar, M., Nisar, K.S., Raja, M.A.Z., Zeb, M., Morsy, A., 2022. The design of intelligent networks for entropy generation in Ree-Eyring dissipative fluid flow system along quartic autocatalysis chemical reactions. Int. Commun. Heat Mass Transf. 133, 105971.
SUS, K.P.P.S.C. and Eastman, J.A., 2002. Mechanisms of heat flow in suspensions of nano-sized particles (nanofluids) Int. J. *Heat Mass Transfer*, *45*(4), pp.855-863.
Tabbussum, R., Dar, A.Q., 2021. Performance evaluation of artificial intelligence paradigms—artificial neural networks, fuzzy logic, and adaptive neuro-fuzzy inference system for flood prediction. Environ. Sci. Pollut. Res. 28 (20), 25265–25282.
Vassallo, P., Kumar, R., D'Amico, S., 2004. Pool boiling heat transfer experiments in silica–water nano-fluids. Int. J. Heat Mass Transf. 47 (2), 407–411.
Vemulawada, S., Jayavel, P., Verma, A., Ghachem, K., Kolsi, L. and Ramesh, K., 2023. Thermal analysis on electromagnetic regulated peristaltic blood-based graphane/diamond nanofluid flow with entropy optimization. *Numerical Heat Transfer, Part B: Fundamentals*, pp.1-25.
Yang, J.Y., Ma, W.X., Khalique, C.M., 2020. Determining lump solutions for a combined soliton equation in (2+ 1)-dimensions. Eur. Phys. J. Plus 135 (6), 1–13.
Zhang, J., Liu, A., Liang, D., Chen, X. and Gao, M., 2021. Interpatient ECG Heartbeat Classification with an Adversarial Convolutional Neural Network. *Journal of Healthcare Engineering*, *2021*.